Optica Applicata, Vol. XLIV, No. 3, 2014
DOI: 10.5277/oa140310

Luminescence of hydrothermally fabricated $PbF_2:Er^{3+}$ particles and their application in bifacial silicon solar cells

FANG YANG[1], CHENYANG WU[2], XIULI HAO[1], YONGSHENG CHEN[1*], JINGXIAO LU[1], SHI-E YANG[1]

[1]Key Lab of Material Physics, Department of Physics, Zhengzhou University, Zhengzhou 450052, China

[2]Yingli Solar, 3399 Chaoyang North Road, Baoding, China

We report the synthesis of $PbF_2:Er^{3+}$ particles using a hydrothermal method. The structure and upconversion emission properties of the products are investigated by scanning electron microscopy, X-ray diffractometer, Raman spectrophotometer and fluorescence spectrometry. An increase in Er^{3+} concentration in the crystals changes the PbF_2 structure from a mixed phase to a cubic phase and decreases the grain size to nanoscale levels. Enhanced upconversion efficiency is achieved after annealing resulted from the formation of the cubic phase and the increase of grain size. The optimal Er^{3+} concentration is found to be 4% after annealing, and applied to the back of a bifacial silicon solar cell, maximum external quantum efficiencies of 0.38% and 0.79% are respectively obtained under 0.77 W/cm^2 laser excitation (1560 nm) and AM1.5 + laser co-excitation.

Keywords: $PbF_2:Er^{3+}$ particles, hydrothermal method, upconversion.

1. Introduction

The upconversion (UC) luminescence of lanthanide-doped fluorides has attracted significant attention because of their low phonon energy and good optical performance [1–3]; these fluorides are widely used in lasers, sensors, and fluorescence bimolecular markers [4–6]. PbF_2, a highly transparent material that allows a wide range of light to pass through it without much attenuation in luminescence, has many advantages as a host matrix for Ln^{3+} ions. The phonon energy of PbF_2 is <250 cm^{-1}, which is significantly lower than that of $NaYF_4$ (~360 cm^{-1}) [7]. In addition, PbF_2 undergoes orthorhombic (α) to cubic (β) phase transition at temperatures >335°C, a characteristic that makes the material an interesting subject for structure-property studies [8].

Many investigations on lanthanide-doped transparent glass ceramics containing PbF_2 nanocrystals have been reported [7, 9–11]; in these reports, doping of PbF_2 and glass ceramic formation are simultaneously completed using PbF_2 and LnF_3 or Ln_2O_3 as raw materials and Ln^{3+}-doped PbF_2 nanoparticle synthesis through chemical etching

of the bulk glass ceramics. In 2010, GANGQIANG ZHU *et al*. [12] reported the fabrication of PbF_2 microstructures via a simple hydrothermal method and found that treatment time, amount of cetyltrimethyl ammonium bromide used, and F/Pb molar ratio significantly affect the resultant PbF_2 shape and phase structures. SARKAR *et al*. [13] reported the synthesis of PbF_2:Dy^{3+} nanocrystals by a hydrothermal method. In the present study, we fabricate PbF_2:Er^{3+} nanoparticles using a hydrothermal method and investigate the effects of doping concentration and high-temperature annealing on the luminescence properties of the products. The fabricated materials are then applied to a bifacial silicon (c-Si) solar cell, and improvements in near-infrared responses are discussed.

2. Experiment

Er_2O_3 was dissolved in dilute HNO_3 (1:1 volume ratio) with heating and stirring to prepare an $Er(NO_3)_3$ stock solution (0.1 mol/dm^3). A certain amount of $Pb(C_2H_3O_2)_2$ was dissolved in 5 cm^3 of deionized water. After mixing these two solutions at different Er^{3+} to Pb^{2+} mole ratios, NH_4HF_2 solution was gradually added to the mixture to form a white suspension. A certain amount of citric acid was then added to the white suspension. The resulting solution was stirred for approximately 10 min and then transferred into a 100 cm^3 Teflon vessel. The vessel was filled with deionized water up to 60% of the total volume and then sealed tightly. Thereafter, the solution was heated at 200°C for 8 h and then slowly cooled to room temperature. The solution was centrifuged, and the obtained products were thoroughly washed with deionized water and dehydrated alcohol. The products were dried in air at approximately 100°C for 2 h. To improve the emission intensity of the product, high-temperature annealing was implemented for 1 h.

The crystalline structure and morphologies of the products were characterized using a scanning electron microscope with an energy-dispersive spectrometer (SEM-EDS, JEOL-JSM-6700F/INCA-ENERGY), a transmission electron microscope (TEM, JEM-2100), a Raman spectrophotometer (Renishaw-2000 within the range of 200 to 880 cm^{-1}; the laser source at 514 nm was used as the excitation source, and the laser power level was 5 mW) and an X-ray diffractometer (XRD, Philips PANAlytical X'pert) with Cu Kα radiation. The UC spectra of the products were recorded by a spectrophotometer (Fluoromax-4, Horiba Jobin Yvon) under 1560 nm laser excitation.

A c-Si solar cell with an area of 2.6 cm×2 cm was used to verify the enhanced solar cell response from the UC process. Under AM1.5G illumination (2000AAA, Crowntech, Inc.), the solar cell without phosphor exhibited approximately 20% and 17% efficiency when illuminated from the front and rear, respectively. PbF_2:Er^{3+} powder was attached to the rear of the solar cell by dissolution in cyclohexane and then spin-coating to yield a UC layer thickness of 500 μm. The laser beam was not focused with a diameter of 5 mm, and the intensity was measured using a power meter (VPL-2W, Beijing Viasho Technology Co., Ltd.). The short circuit current of the solar cell was measured using a galvanometer (Keithley, 6517).

3. Results

Representative XRD patterns of the as-prepared samples are shown in Fig. 1. All of the diffraction peaks of the undoped PbF_2 sample can be readily indexed to an orthorhombic (α) phase (JCPDS Card No. 41-1086), and no diffraction peak corresponding to any impurity or allotropic phase is found. By contrast, mixed orthorhombic and cubic (β) phases (JCPDS Card No. 06-0251) are observed in the doped samples. As the Er^{3+} concentration in the crystals is increased, the peaks corresponding to the cubic phase are enhanced whereas those corresponding to the orthorhombic phase are weakened.

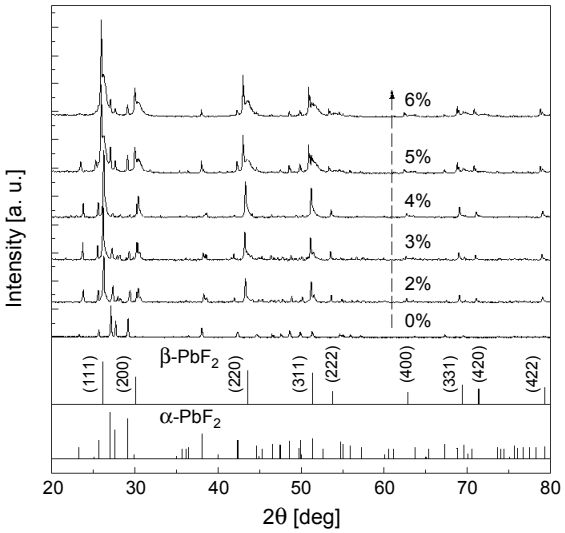

Fig. 1. XRD patterns of samples with different Er^{3+} concentrations.

Typical SEM and TEM images of the samples are shown in Fig. 2. In Fig. 2**a**, the undoped PbF_2 sample shows a spherical form with sizes ranging from 4 to 6 μm. After doping, the size of the particles (Fig. 2**b**) decreases to approximately 100 nm, and an elemental composition including F, Pb, and Er is observed (Fig. 2**c**). TEM images (Fig. 2**d**) also indicate the formation of spherical nanocrystals with sizes between 50 and 100 nm. The diffraction pattern (Fig. 2**e**) corresponds to the face-centered cubic fluorite lattice [14].

The phase transition behavior of PbF_2 has been studied in various experiments using high-pressure and theoretical techniques [12, 15–17]. While phase transition behaviors can be qualitatively explained by Ostwald ripening and oriented attachment [18], these explanations mainly focus on undoped PbF_2 growth conditions. In the current system, the size modification and phase transition caused by Er^{3+} doping originate from the surface charge redistribution of the crystal nucleus, which is induced by inner electron charge transfer between dopant ions and lattice cations [19].

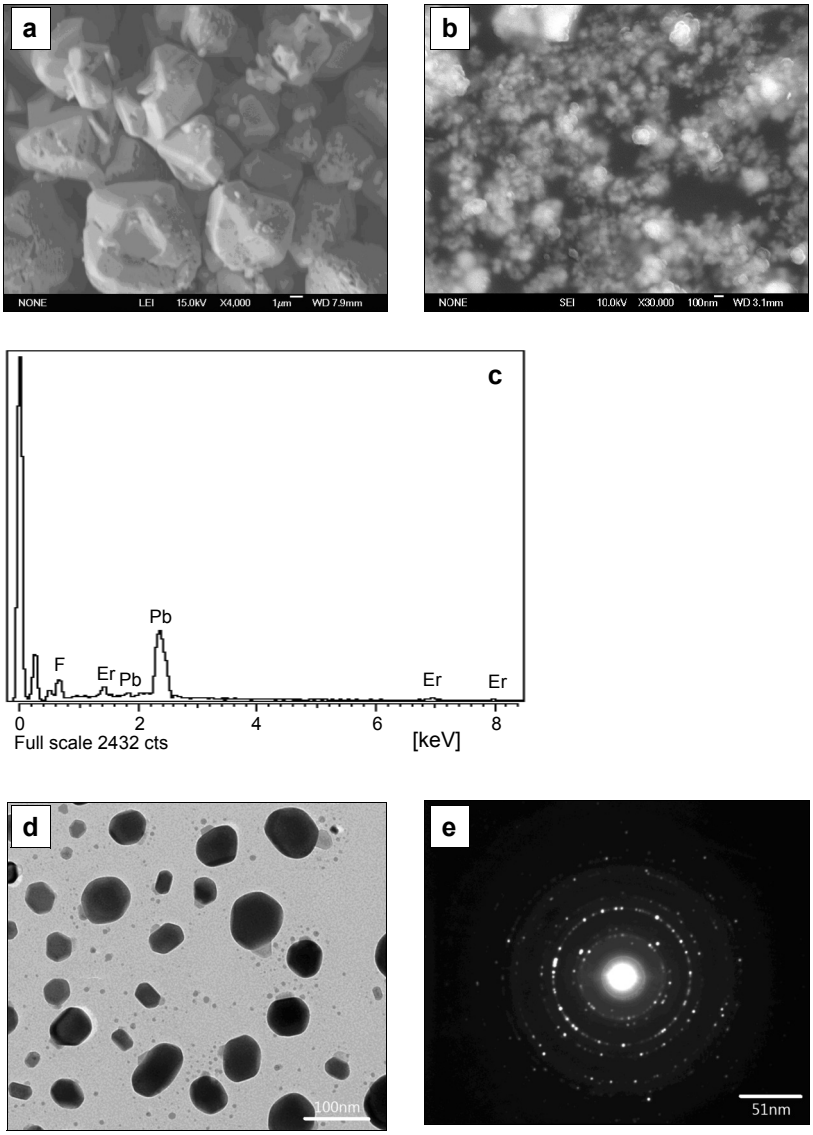

Fig. 2. SEM image of the undoped sample (**a**), SEM (**b**), comparison spectra (**c**), TEM (**d**) and selected area electron diffraction pattern (**e**) of PbF_2:Er(6%) sample.

The upconversion emission spectra of the as-prepared samples excited at 300 mW, 1560 nm laser are presented in Fig. 3. A major infrared emission corresponding to the ${}^4I_{11/2} \rightarrow {}^4I_{15/2}$ Er^{3+} transition is found at 970 nm. Weaker infrared, red, and green emissions, which correspond to ${}^4I_{9/2} \rightarrow {}^4I_{15/2}$, ${}^4F_{9/2} \rightarrow {}^4I_{15/2}$, and ${}^2H_{11/2}({}^4S_{3/2}) \rightarrow {}^4I_{15/2}$ transitions, are found at approximately 800, 650, and 540 nm, respectively. The emission intensity significantly increases with increasing Er^{3+} concentration from 2% to 5%;

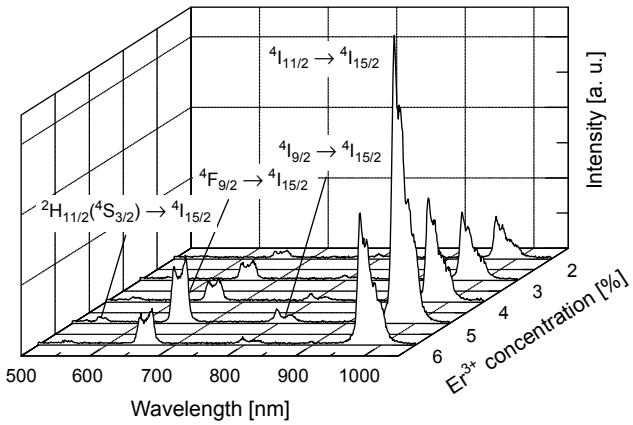

Fig. 3. Er^{3+} concentration-dependent emission intensity of the as-prepared samples.

further increases in Er^{3+} concentration, however, decrease the emission intensity. Therefore, the optimum Er^{3+} doping concentration for the as-prepared samples is 5%.

Upconversion (UC) nanomaterials generally have low emission efficiencies partly because of structural defects, such as interstitial anions and cation vacancies, and partly because of their large surface area, which features various quenchers induced by solvers or surface defects such as absorbed contaminants [20, 21]. Therefore, high-temperature annealing is used to enhance the emission efficiency. The XRD spectra of PbF_2:Er^{3+}(4%) samples annealed under different temperatures for 1 h in air are shown in Fig. 4. The proportion of cubic phase particles increases with increasing annealing temperature, which indicates that the cubic phase is thermodynamically stable. In addition, the full width at half-maximum decreases with increasing annealing temperature, which indicates that the grain size increases after annealing. This finding is demonstrated by the SEM images in Fig. 5. With the increase in annealing temperature,

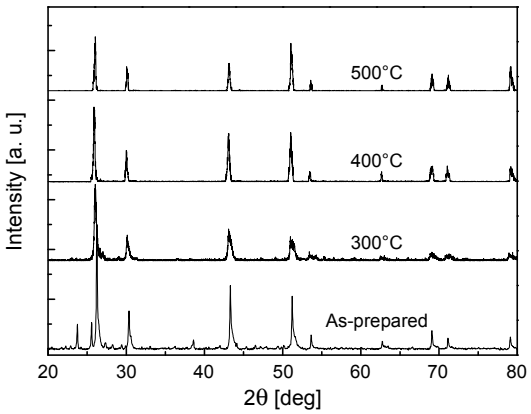

Fig. 4. XRD patterns of the annealed PbF_2:Er^{3+}(4%) samples under different temperature.

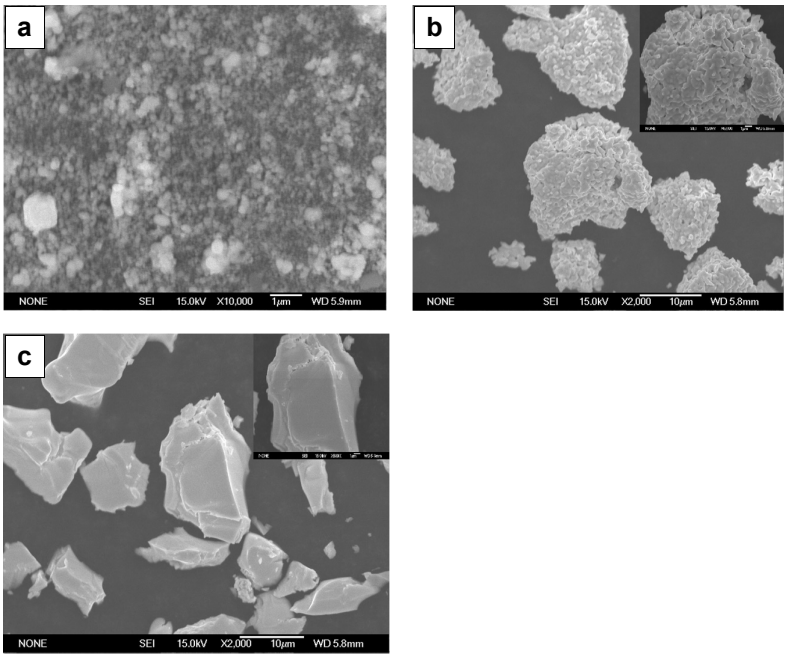

Fig. 5. SEM images of the annealed PbF_2:Er^{3+}(4%) samples under different temperature: 300°C (**a**), 400°C (**b**), and 500°C (**c**).

the grain aggregation occurs and micro-grade particles are formed after annealing at 500°C, which may contribute to the increase in UC emission.

The UC emission spectra of the annealed samples under different temperature are shown in Fig. 6 excited at 60 mW, 1560 nm laser. It is conformed that with the increase in annealing temperature, the UC emission intensity increases due to the increase in

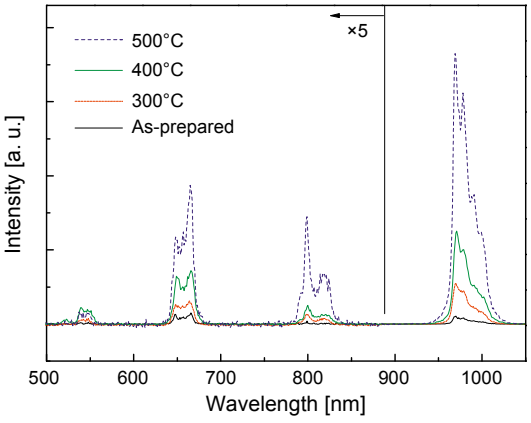

Fig. 6. The UC emission spectra of the annealed PbF_2:Er^{3+}(4%) samples under different temperature. The signals corresponding to the emissions at 540, 650, and 800 nm are amplified 5.0 times.

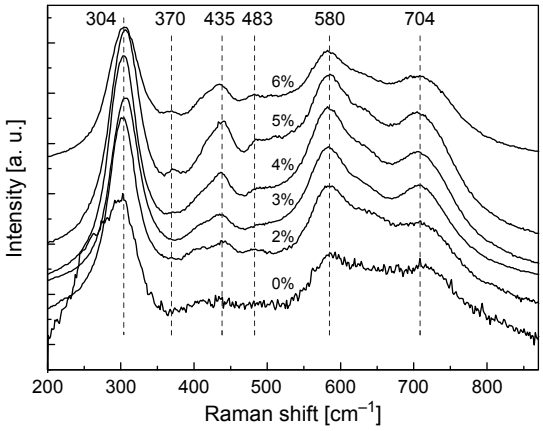

Fig. 7. The Raman spectra of samples annealed at 500°C for 1 h with varying Er^{3+} concentration.

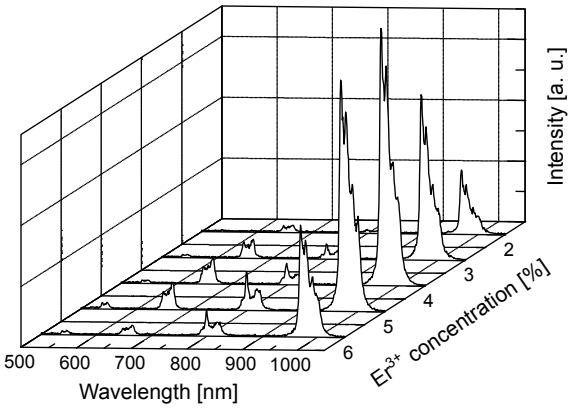

Fig. 8. Emission intensities of samples annealed at 500°C for 1 h with varying Er^{3+} concentration.

the grain size and the formation of the cubic phase. Figure 7 shows the Raman spectra of the samples annealed at 500°C for 1 h with varying Er^{3+} concentration. For the undoped sample, one dominating peak accompanied by three weak and broad peaks are found at about 304, 435, 580, and 704 cm^{-1}, ascribed to the vibrational modes and the presence of electronic centers [22]. With the addition of Er^{3+}, two weak peaks are shown around 370 and 483 cm^{-1}. The emission spectra of the samples annealed at 500°C for 1 h with different doping concentrations are presented in Fig. 8. The variation in emission intensity of samples as a function of Er^{3+} concentration shows the same change tendency as that of as-prepared samples. However, the optimum doping concentration of Er^{3+} decreases to 4%.

The UC emission intensities of the PbF_2:Er^{3+}(4%) sample observed after annealing at 500°C were recorded as a function of excitation power in log–log plots (Fig. 9). The intensities of the green, red, and infrared emissions increase with increasing excitation power and eventually reach saturation. The slope of the infrared emission is

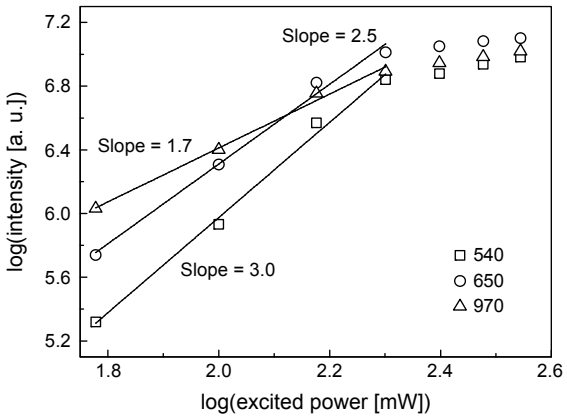

Fig. 9. Excitation power-dependent UC intensities of the PbF_2:Er^{3+}(4%) sample after annealing at 500°C.

approximately 2 under low pumping power, indicating a well-known two-photon mechanism. In addition, the slopes of the green and red emissions are approximately 3, corresponding to a three-photon emission process.

The PbF_2:Er^{3+}(4%) powders annealed at 500°C for 1 h were applied to the rear of the c-Si solar cell with a typical bandgap of 1.1 eV. The log–log plot of the short-circuit current as a function of excitation power is shown in Fig. 10. Similar to the UC emissions shown in Fig. 9, the short-circuit current increases with increasing excitation power and reaches saturation, thereby indicating a direct relationship between the currents and the UC emission intensities. The slope of the short-circuit current under low power is similar to that of infrared emission, which suggests that the photon-generated carriers are derived mainly from infrared excitation. The external quantum efficiency (EQE) of the solar cell, which is defined as the ratio between the number of generated electron–hole pairs caused by the UC emission and the number of incident infrared photons, can be calculated as follows [23]:

$$\mathrm{EQE} = \frac{I_{\mathrm{sc}}}{P_{\mathrm{in}}\, q / h\gamma}$$

where I_{sc} is the short-circuit current, q is the electron charge, P_{in} is the excitation power, and $h\gamma$ is the energy of the laser photon. The calculated EQE values with the corresponding excitation power are presented in Fig. 10. EQE increases with increasing, reaches a maximum (0.38%) at 150 mW (0.77 W/cm^2), and then decreases with further increases in excitation power because of I_{sc} saturation. This maximum value is comparable with reported values obtained at 2305 W/m^2 for $NaYF_4$:Er^{3+}(20%) in a c-Si solar cell system at 1523 nm (0.64%) [24] and at 37 mW (235 μm×235 μm) for Er^{3+}-Yb^{3+} co-doped fluoroindate glasses at 1480 nm (0.4%) [25]. Therefore, PbF_2 is an excellent host material for high-efficiency UC processes.

In actual application processes, photons from sun irradiation and UC emission are absorbed simultaneously by solar cells. Thus, the response of solar cells under this con-

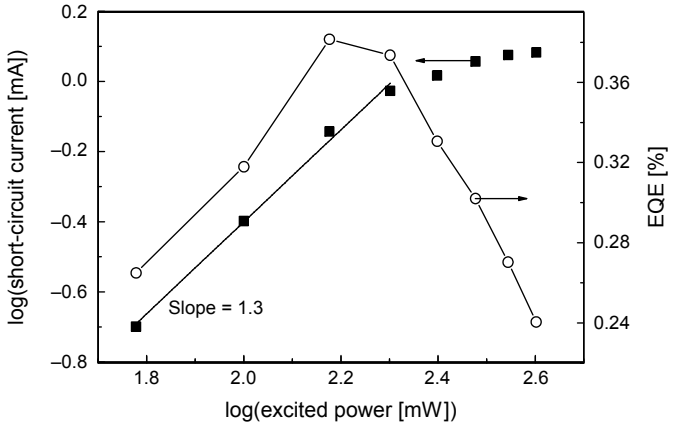

Fig. 10. Log–log diagrams of short-circuit current and the EQE as a function of excitation power.

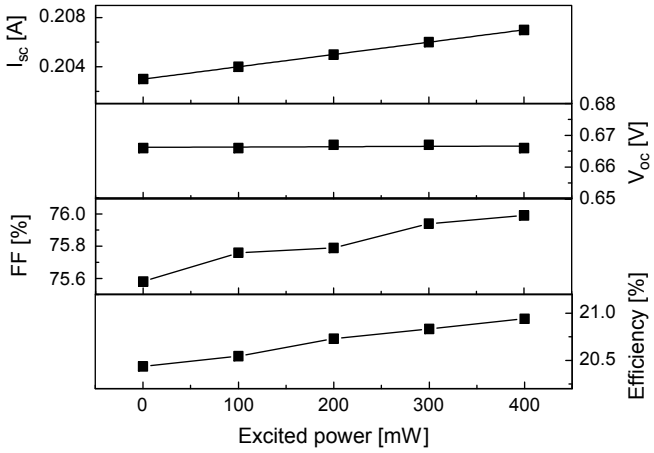

Fig. 11. Solar cell properties as a function of excitation power at 1560 nm under co-excitation condition.

dition differs significantly from that observed under laser excitation only. However, to the best of our knowledge, few experiments and theoretical calculations have studied this difference [1]. The influence of laser power on the properties of c-Si (E_g = 1.12 eV) solar cells under AM1.5 and laser co-excitation was evaluated (Fig. 11); here, all of the incident lights are perpendicular to the solar cell and the UC layer. The open-circuit voltage V_{oc} remains nearly constant with increasing power because of the logarithmic dependence on light intensity. I_{sc} increases linearly with increasing laser power, and an EQE of 0.79% may be obtained, which is higher than the 0.38% shown in Fig. 10. This result is due to the saturation of carrier recombination under co-excitation, which enhances the collection of electron–hole pairs generated by UC emissions and leads to an increase in a fill factor. Therefore, the efficiency of the solar cell increases with increasing laser power, and 0.5% enhancement is achieved at 400 mW.

4. Conclusions

PbF_2:Er^{3+} particles are synthesized in this study using a hydrothermal method. Transformation from the mixed phase to cubic phase occurs with increasing dopant concentration, and high-temperature annealing contributes to the formation of the cubic phase and the increase in the grain size as well as improvements in UC emission. The optimal doping concentration (4%) is obtained after annealing. When the PbF_2:Er^{3+}(4%) particles are applied in c-Si solar cells, a maximum EQE of 0.38% is achieved under 150 mW, 1560 nm excitation. However, under co-excitation with AM1.5 and laser irradiation, an EQE of 0.79% is obtained, resulting in a 0.5% enhancement in efficiency at 400 mW excitation power. The results of this study indicate that PbF_2 is a good candidate host material for UC applications.

Acknowledgements – This work was supported by the National Key Basic Research Program of China (2011CBA00706).

References

[1] TRUPKE T., GREEN M.A., WÜRFEL P., *Improving solar cell efficiencies by up-conversion of sub-band-gap light*, Journal of Applied Physics **92**(7), 2002, pp. 4117–4122.

[2] RODRÍGUEZ V.D., TIKHOMIROV V.K., MÉNDEZ-RAMOS J., DEL-CASTILLO J., GÖRLLER-WALRAND C., *Measurement of quantum yield of up-conversion luminescence in Er^{3+}-doped nano-glass-ceramics*, Journal of Nanoscience and Nanotechnology **9**(3), 2009, pp. 2072–2075.

[3] SONGJUN ZENG, GUOZHONG REN, CHANGFU XU, *Intense blue photoluminescence of the Tm^{3+}/Yb^{3+} co-doped single-crystalline hexagonal phase $NaYF_4$ nanorods*, Journal of Alloys and Compounds **509**(5), 2011, pp. 2540–2543.

[4] NGUYEN D.C., FAULKER G.E., DULICK M., *Blue-green (450-nm) upconversion Tm^{3+}:YLF laser*, Applied Optics **28**(17), 1989, pp. 3553–3555.

[5] DOWNING E.A., HESSELINK L., MACFARLANE R.M., KLEIN J.R., EVANS D., RALSTON J., *A laser-diode--driven, three-color, solid-state 3-D display*, [In] *Summaries of papers presented at the Conference on Lasers and Electro-Optics, CLEO '96*, Vol. 9, 1996, pp. 89–90.

[6] GUANGSHUN YI , HUACHANG LU, SHUYING ZHAO, YUE GE, WENJUN YANG, DEPU CHEN, LIANG-HONG GUO, *Synthesis, characterization, and biological application of size-controlled nanocrystalline $NaYF_4$:Yb, Er infrared-to-visible up-conversion phosphors*, Nano Letters **4**(11), 2004, pp. 2191–2196.

[7] TIKHOMIROV V.K., ADAMO G., NIKOLAENKO A.E., RODRIGUEZ V.D., GREDIN P., MORTIER M., ZHELUDEV N.I., MOSHCHALKOV V.V., *Cathodo- and photoluminescence in Yb^{3+}-Er^{3+} co-doped PbF_2 nanoparticles*, Optics Express **18**(9), 2010, pp. 8836–8846.

[8] PORTELLA K.F., RATTMANN K.R., DE SOUZA G.P., GARCIA C.M., CANTAO M.P., MUCCILLO R., *Characterization of $\alpha \leftrightarrow \beta$ PbF_2 phase transition by several techniques*, Journal of Materials Science **35**(13), 2000, pp. 3263–3268.

[9] FANQING ZENG, GUOZHONG REN, XIANNIAN QIU, QIBIN YANG, JINGWU CHEN, *The effect of PbF_2 content on the microstructure and upconversion luminescence of Er^{3+}-doped SiO_2-PbF_2-PbO glass ceramics*, Journal of Non-Crystalline Solids **354**(29), 2008, pp. 3428–3432.

[10] SILVA M.A.P., BRIOIS V., POULAIN M., MESSADDEQ Y., RIBEIRO S.J.L., *SiO_2-PbF_2-CdF_2 glasses and glass ceramics*, Journal of Physics and Chemistry of Solids **64**(1), 2003, pp. 95–105.

[11] MORTIER M., *Nucleation and anionic environment of Er^{3+} in a germanate glass*, Journal of Non-Crystalline Solids **318**(1–2), 2003, pp. 56–62.

[12] GANGQIANG ZHU, PENG LIU, HOJAMBERDIEV M., JIAN-PING ZHOU, XIJIN HUANG, *Synthesis of orthorhombic and cubic PbF_2 by hydrothermal method*, Journal of Materials Science **45**(7), 2010, pp. 1846–1853.

[13] SARKAR S., HAZRA C., CHATTI M., SUDARSAN V., MAHALINGAM V., *Enhanced quantum efficiency for Dy^{3+} emissions in water dispersible PbF_2 nanocrystals*, RSC Advances **2**(22), 2012, pp. 8269–8272.

[14] TIKHOMIROV V.K., MORTIER M., GREDIN P., PATRIARCHE G., GÖRLLER-WALRAND C., MOSHCHALKOV V.V., *Preparation and up-conversion luminescence of 8 nm rare-earth doped fluoride nanoparticles*, Optics Express **16**(19), 2008, pp. 14544–14549.

[15] EHM L., KNORR K., MÄDLER F., VOIGTLÄNDER H., BUSETTO E., CASSETTA A., LAUSI A., WINKLER B., *High-pressure X-ray diffraction study on α-PbF_2*, Journal of Physics and Chemistry of Solids **64**(6), 2003, pp. 919–925.

[16] ALOV D.L., RYBCHENKO S.I., *Luminescence of orthorhombic PbF_2*, Journal of Physics: Condensed Matter **7**(7), 1995, pp. 1475–1482.

[17] THANGADURAI P., RAMASAMY S., KESAVAMOORTHY R., *Raman studies in nanocrystalline lead (II) fluoride*, Journal of Physics: Condensed Matter **17**(6), 2005, pp. 863–874.

[18] GILBERT B., HENGZHONG ZHANG, FENG HUANG, FINNEGAN M.P., WAYCHUNAS G.A., BANFIELD J.F., *Special phase transformation and crystal growth pathways observed in nanoparticles*, Geochemical Transactions **4**, 2003, p. 21.

[19] XIANGFU WANG, YANYAN BU, YANG XIAO, CAIXIA KAN, DI LU, XIAOHONG YAN, *Size and shape modifications, phase transition, and enhanced luminescence of fluoride nanocrystals induced by doping*, Journal of Materials Chemistry C **1**(18), 2013, pp. 3158–3166.

[20] FENG WANG, JUAN WANG, XIAOGANG LIU, *Direct evidence of a surface quenching effect on size-dependent luminescence of upconversion nanoparticles*, Angewandte Chemie International Edition **49**(41), 2010, pp. 7456–7460.

[21] FENG WANG, XIAOGANG LIU, *Recent advances in the chemistry of lanthanide-doped upconversion nanocrystals*, Chemical Society Reviews **38**(4), 2009, pp. 976–989.

[22] RAMASAMY S., SMITH D.J., THANGADURAI P., RAVICHANDRAN K., PRAKASH T., PADMAPRASAD K., SABARINATHAN V., *Recent study of nanomaterials prepared by inert gas condensation using ultra high vacuum chamber*, Pramana – Journal of Physics **65**(5), 2005, pp. 881–891.

[23] DE WILD J., RATH J.K., MEIJERINK A., VAN SARK W.G.J.H.M., SCHROPP R.E.I., *Enhanced near-infrared response of a-Si:H solar cells with β-NaYF4:Yb^{3+} (18%), Er^{3+} (2%) upconversion phosphors*, Solar Energy Materials and Solar Cells **94**(12), 2010, pp. 2395–2398.

[24] GOLDSCHMIDT J.C., FISCHER S., LÖPER P., KRÄMER K.W., BINER D., HERMLE M., GLUNZ S.W., *Experimental analysis of upconversion with both coherent monochromatic irradiation and broad spectrum illumination*, Solar Energy Materials and Solar Cells **95**(7), 2011, pp. 1960–1963.

[25] HERNÁNDEZ-RODRÍGUEZ M.A., IMANIEH M.H., MARTÍN L.L., MARTÍN I.R., *Experimental enhancement of the photocurrent in a solar cell using upconversion process in fluoroindate glasses exciting at 1480 nm*, Solar Energy Materials and Solar Cells **116**, 2013, pp. 171–175.

Received February 13, 2014
in revised form April 8, 2014